Sweet Ionic Liquids as High-Temperature and High-Voltage Supercapacitor Electrolytes

N.B. When citing this work, cite the original published paper.

(article starts on next page)

Sweet Ionic Liquids as High-Temperature and High-Voltage Supercapacitor Electrolytes

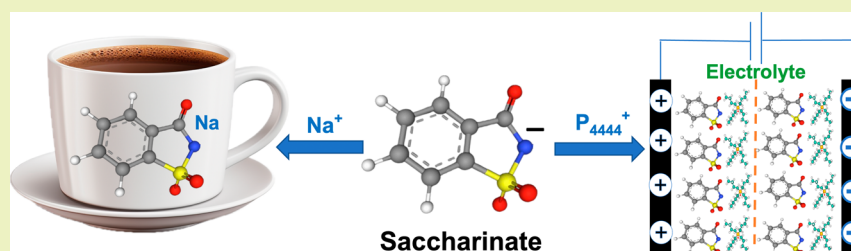Mukhtiar Ahmed, Gaurav Tatrari, Patrik Johansson,* and Faiz Ullah Shah*

ACCESS | Metrics & More | Article Recommendations | Supporting Information

ABSTRACT: We here present four new fluorine-free ionic liquids (ILs) based on the non-nutritive sweetener saccharinate (Sac) anion coupled with pyrrolidinium, imidazolium, and phosphonium cations and their thermal, physicochemical, and electrochemical properties. The pyrrolidinium cation-based material is a solid at room temperature, whereas the other three materials are room-temperature ionic liquids (RTILs). By infrared spectroscopy, we find the ionic interactions to be controlled by the distinct conformers of the Sac anion, which in turn are cation-dependent. $(P_{4444})(Sac)$ shows the lowest glass transition temperature, (T_g), the highest thermal stability and ionic conductivity, and the widest electrochemical stability window, up to 6 V. As an electrolyte in a symmetric supercapacitor, it enabled a specific capacitance of 204 F g^{-1} at 1 mV s^{-1}, an energy density of 53 Wh kg^{-1} and a power density of 300 W kg^{-1} at a current density of 0.1 A g^{-1}, and the capacitor retained 81% of its initial capacitance after 10,000 cycles at 60 °C. Altogether, these fluorine-free electrolytes have electrochemical properties promising for application in supercapacitors operating at elevated temperatures over a wide voltage range.

KEYWORDS: saccharinate, sweet ionic liquids, electrolytes, electrochemistry, supercapacitors

INTRODUCTION

Ionic liquids (ILs) are by definition organic or inorganic—organic hybrid salts with melting points below 100 °C and possess a combination of interesting properties.[1] ILs are interesting as solvents and/or electrolytes,[2,3] due to their very low to negligible vapor pressures, high boiling and low melting points, wide liquid phase ranges, a highly ionic environment, synthetic diversity, and their "greener" nature.[4,5] However, not all ILs are green,[6,7] especially as the commonly used fluorinated anions demand cumbersome synthesis and furthermore can release hazardous hydrofluoric acid (HF) and other fluorinated species,[8] which can pollute the surrounding environment and may cause severe environmental and health issues.

Electric double-layer capacitors (EDLCs), also known as supercapacitors or ultracapacitors, have gained interest due to their power delivery capability, bridging the gap between dielectric capacitors and batteries—and this way connects to being "green"—by enabling better use of fossil free technologies.[9] Conventional EDLCs are based on aqueous electrolytes that have rather narrow electrochemical stability windows (ESWs)—which limits the energy density, while wider ESW organic electrolytes[10] have several other drawbacks:

toxicity, flammability, and corrosiveness.[11] ILs with their often even wider ESWs should eventually be able to successfully replace these and then ideally be based on fluorine-free anions, such as aromatic or aliphatic carboxylates,[12,13] phosphates,[14,15] sulfates,[16,17] or orthoborates.[18] However, carboxylate and sulfate anions are highly basic, and their ILs have low ionic conductivities, while the phosphate anion-based ILs are too expensive and also have limited ionic conductivities. On the other hand, many of the orthoborate ILs are hydrolytically unstable with limited ESWs.
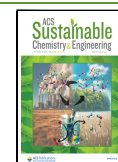
In general, the low ionic conductivity and high viscosity may, however, limit the power performance of EDLCs based on ILs at ambient temperature. One possible remedy is to create hybrid IL-organic solvent-based electrolytes, but these are unsuitable for applications where the operating temperatures exceed 50 °C.[19] Additionally, acetonitrile, the most common

EDLC organic solvent, may in fact decrease the ionic conductivity of ILs by promoting ion−ion association.[20] Another route is to use elevated temperatures to increase the ionicity. In a previous study, we demonstrated ca. five times higher energy and power densities by increasing the operating temperature from 20 to 100 °C using an IL electrolyte, tetra(*n*-butyl)phosphonium furoate (P_{4444})(FuA).[12]

Here, we exploit the fluorine-free saccharinate (Sac) anion to form ILs, an anion which has been extensively used as non-nutritive sweetener with well-established toxicity essays.[21] ILs based on Sac were first reported by Davis, Jr. et al.,[4] and these exhibit properties that, in several aspects, closely resemble those of the structurally similar 2,2,2-trifluoro-*N*-(trifluoromethylsulfonyl) acetamide (TSAC)[22] and bis-(trifluoromethanesulfonyl)imide (TFSI),[23] but heavily fluorinated anions. For example, in terms of hydrogen bonding capability and basicity, and weak metal coordination and ionic interactions, all this combined provides similar transport properties.[4,24]

Despite their structural similarity to TFSI- and TSAC-based ILs, the saccharinate-based ILs reported to date remain less diverse compared with their fluorinated counterparts. While extensive research has been devoted to the properties and applications of fluorinated ILs, created through various combinations of cations and anions, only a limited number of reports are available on fluorine-free ILs. In this study, we aim to thoroughly investigate the physicochemical and electrochemical properties of saccharinate-based ILs with different cations, including pyrrolidinium, imidazolium, and phosphonium, and to explore the application of one selected IL as an electrolyte in electrochemical EDLCs. We expect the fluorine-free ILs based on Sac to be able to improve safety and sustainability, not only at the synthesis and supercapacitor application stages but also within the recycling processes.[25,26] Furthermore, the compact Hückel-type aromatic structure of Sac, as shown to be a viable path to create new anions suitable for electrochemical applications,[27,28] can potentially offer ILs with improved thermal, transport, and electrochemical properties. All of these properties are systematically investigated for all four ILs, alongside the performance of the most promising IL in a symmetric multiwalled carbon nanotube (MWCNT)-based supercapacitor, operating also at elevated temperatures.

■ EXPERIMENTAL SECTION

Materials and Synthesis. Unless otherwise stated, all commercial reagents were used without any additional purification. Methylimidazole (ACS reagents, >97% purity), 1,2-dimethylimidazole (ACS reagents, >97% purity), methylpyrrolidine (ACS reagents, >97% purity), sodium saccharine (>99% purity), *n*-tetrabutylphosphonium bromide (>98% purity), *N*-methyl-2-pyrrolidone (NMP) (anhydrous, 99.5% purity), polyvinylidene fluoride (PVDF) (>99% purity), and activated carbon were received from Sigma−Aldrich. Sodium sulfate (anhydrous, 99% purity), dichloromethane (DCM) (96% purity), and diethyl ether (≥99.5% purity by GC, stabilized) were purchased from VWR (BDH) chemicals. Battery-grade aluminum foil was purchased from Cambridge Energy Solutions Ltd.

All ILs were synthesized through a simple metathesis reaction. The equivalent amount of bromide salts[29] and sodium saccharine was separately dissolved in milli-Q water, mixed slowly, and continuously stirred for 24 h at ambient temperature. The products were extracted with 50 mL of DCM thrice, and the organic layer with the IL product was separated and dried over anhydrous sodium sulfate. DCM was evaporated under vacuum at elevated temperature, and the product obtained was washed with diethyl ether and dried under vacuum at 80 °C for at least 4 days. The absence of bromide was confirmed by

treating the final IL products with aqueous $AgNO_3$ solution. The water contents were measured by Karl Fischer titration (using a Metrohm 917 Coulometer, Switzerland); the values are given in Table 1. All ILs were separated in ca. quantitative yield. The purity of the ILs was confirmed by ^1H and ^{13}C nuclear magnetic resonance (NMR) spectroscopy.

Table 1. Physico-Chemical and Electrochemical Properties[a]

system	water content (±5 ppm)	T_m (°C)	T_g (°C)	T_d (°C)	σ at 30 °C (S cm^{-1})	ESW (V)
(MBPyrr) (Sac)	45	34	−32[b]	261		
(P_{4444})(Sac)	17		−44	381	2.5×10^{-4}	6.0
(MBIm) (Sac)	57		−34	277	5.9×10^{-4}	4.2
(MMBIm) (Sac)	38		−30	293	1.3×10^{-4}	4.5

[a]T_m, melting temperature; T_g, glass transition temperature; T_d, decomposition temperature; and σ, ionic conductivity. [b]Second heating cycle.

Electrode and Supercapacitor Preparation. The electrode materials were prepared using MWCNTs (>95% carbon basis) purchased from Sigma-Aldrich, with diameters ranging from 50 to 90 nm. The binder solution was prepared by dissolving 20 mg of PVDF in 20 mL of NMP and agitating the mixture overnight on a magnetic stirrer plate at a temperature of 40 °C. Twenty milligrams of activated carbon (with a particle size less than 90 nm) was combined with 160 mg of MWCNT and continuously ground using a mortar grinder for about 30 min to produce a uniformly sized powder. The binder solution was gradually added to the powder while being combined with a mortar grinder until a uniform slurry was obtained.

A battery-grade aluminum foil, to be used as substrate, was thoroughly purified using acetone and thereafter placed in a vacuum oven for 1 h before being used. The coating process then used the Doctor's blade method to evenly distribute the slurry with a thickness of 150 mm. The electrodes were placed in a vacuum oven at 60 °C and 200 mbar for 2 days. Subsequently, supercapacitors were constructed using two identical MWCNT electrodes with 14 mm diameter and 0.2 mm thickness separated by a Whatman filter paper (G/FD grade) separator, which was vacuum-sealed at room temperature in order to improve the wetting/absorption of the IL electrolyte into its pores. Finally, the assembly was placed in a CR 2032 coin cell case.

NMR Spectroscopy. The structures and purity of all produced compounds were validated using a Bruker Ascend Aeon WB 400 NMR spectrometer (Bruker BioSpin AG, Fallanden, Switzerland), with operating frequencies of 400.21 MHz for ^1H, 100.64 MHz for ^{13}C, and 162.01 MHz for ^{31}P. CDCl$_3$ was employed as a solvent, and Bruker Topspin 3.5 software was used to process the data.

Thermal Analysis. Thermogravimetric analysis (TGA) was performed using a PerkinElmer TGA 8000 under N_2 gas at the heating rate of 10 °C per min with 2−4 mg of sample for each experiment. The onset of decomposition temperature, T_{onset}, was computed as the junction of the baseline weight and the tangent of the weight vs temperature with the help of the Pyris software. PerkinElmer DSC 6000 instrument was used to record the differential scanning calorimetry (DSC) traces, both cooling and heating, with 2−5 mg of the material deposited in an aluminum pan at the scanning rates of 2 and 5 °C min^{-1}. The inert atmosphere inside the sample chamber was maintained with a steady flow of dry nitrogen at a flow rate of 20 mL min^{-1}. The glass transition temperature, T_g, was calculated from the inflection midpoint of the original S-shaped transition slope with the help of the Pyris software.

Electrochemical Characterization. The electrochemical properties were assessed using a Metrohm Autolab PGSTAT302N electrochemical workstation with an FRA32 M module for impedance measurements controlled by Nova 2.02 software. About 70 μL of the

sample was packed in a TSC 70 cell coupled to a Microcell HC from rhd Instruments, Germany. Three-electrode setup was employed for linear sweep voltammetry (LSV) experiments: a glassy carbon (GC) wire with a diameter of 2 mm as the working electrode (WE), Pt crucible as a counter electrode (CE) as well as a sample container, and the pseudoreference electrode, a Ag wire coated in AgCl was used as a reference electrode (RE). Both cathodic and anodic scans were recorded at a scan rate of 1 mV s^{-1} at 20 °C temperature. The electrochemical potentials were calibrated by using ferrocene (Fc) as an internal reference. The ESW limits were defined by a 0.1 mA cm^{-2} cutoff current density.

The ionic conductivity was determined by impedance measurements with a frequency range of 1 Hz to 1 MHz and an AC voltage amplitude of 10 mV. All the impedance spectra were recorded during heating and cooling at temperatures from −20 to 100 °C. A two-electrode system was used for ionic conductivity studies using GC as the WE and a Pt crucible as the CE and sample container. For the room-temperature solid salt, a TSC battery cell with stainless steel discs as current collectors was used. To adjust the thickness of the film, a 0.2 mm spacer interposed between the two-disc electrodes (Kcell = 0.039789 25 cm^{-1}) was used. Prior to measurements, the solid sample was kept at 100 °C for 30 min, followed by cooling to ambient temperature.

The ionic conductivities of the RTILs were further analyzed by fitting the ionic conductivity data to the Vogel−Fulcher−Tammann (VFT) eq 1.[30]

$$\sigma = \sigma_0 \exp\left(\frac{-B}{(T - T_0)}\right) \tag{1}$$

where σ_0 is a pre-exponential factor, B and T_0 are adjustable parameters, where the former is an empirical fitting parameter related to T_g and activation energy (E_σ) of the system, and the latter is referred to as the ideal glass transition temperature where the configurational entropy vanishes.

Both electrodes were polished with 0.25 m of Kemet diamond paste before each LSV and ionic conductivity measurement. A Metrohm 100 S cm^{-1} KCl standard solution was used to compute the cell constant (Kcell = 1.8736 cm^{-1}). The cell was thermally equilibrated before recording the impedance spectra for 10 min.

The supercapacitor coin cells were tested by using a Biologic BCS-810 battery cycler equipped with an impedance module. The electrochemical properties were evaluated by using cyclic voltammetry (CV), galvanostatic charge−discharge (GCD) cycling, and electrochemical impedance spectroscopy (EIS). Initially, CV was performed at 50 mVs^{-1} with a potential window of 2 V to test the feasibility, stability, and reversibility of each cell. Then, CV was performed at different scan rates from 1 to 200 mV s^{-1} over potential windows of 2 and 4 V at two different temperatures of 30 and 60 °C. EIS was performed in the frequency range from 0.01 Hz to 10^6 Hz, and GCD was performed at different current densities of 0.1, 0.2, 0.3, 0.4, and 1 A g^{-1} over a potential window of 2 V. All the electrochemical experiments were performed inside a temperature-controlled climate chamber. The specific capacitance (C_s) was calculated from the CV and GCD data using eqs 2 and 3, respectively.[31,32]

$$C_s = \frac{\int i \, dV}{2mK\Delta V} \tag{2}$$

$$C_s = \frac{i\Delta t}{m\Delta V} \tag{3}$$

where C_s is the specific capacitance in F g^{-1}, $\int i \, dV$ is the area under the curve, m is the mass in mg (1.5 mg for each electrode), K is the scan rate in mV s^{-1}, Δt is the discharge time, ΔV is the potential window in V, and i is the current in mA.[31] Finally, the energy density (E_D) (in Wh kg^{-1}) and power density (P_D) (in W kg^{-1}) were evaluated using eqs 4 and 5, respectively.[31]

$$E_D = \frac{CV^2}{3 \cdot 6 \times 2} \tag{4}$$

$$P_D = \frac{E_D \times 3600}{\Delta t} \tag{5}$$

The long-term stability was performed using a current density of 1 A g^{-1} up to 5000 and 10,000 charge−discharge cycles at 30 and 60 °C, respectively.

Attenuated Total Reflection−Fourier Transform Infrared Spectroscopy. Attenuated total reflection−Fourier transform infrared (ATR-FTIR) spectra were acquired utilizing the double-side forward−backward acquisition mode on a Bruker IFS 80v spectrometer outfitted with a deuterated triglycine sulfate (DTGS) detector and diamond ATR attachment. 256 scans were coadded and signal-averaged at an optical resolution of 4 cm^{-1}.

■ RESULTS AND DISCUSSION

We start with the synthesis and structural characterization of the ILs, followed by outlining their thermal behavior and transport properties. We then progress to the ATR-FTIR study to address the ionic interactions in detail, and finally, we present the systematic electrochemical assessment under different conditions for one selected IL, (P$_{4444}$)(Sac), used in a symmetric supercapacitor.

Basics of Synthesis. The fluorine-free ILs were created by a simple metathesis reaction at ambient temperature using water as a solvent. The "onium" bromide salts are mixed with sodium saccharine, and the products are produced in a single-step reaction from readily available and relatively low-cost starting materials. The resulting (MBPyrr)(Sac) is a solid at ambient temperature, while the other three salts are RTILs. Each IL was checked for residual bromide using AgNO$_3$, and those with a positive test were repeatedly extracted with dichloromethane and dry acetone until the complete removal of bromide contents. These nonfluorinated ILs are greener, cost-effective and easy to synthesize from readily available precursors. Unlike the fluorinated analogues, which are sensitive to moisture, prone to hydrolysis, corrosive to metals, and expensive to produce, these fluorine-free ILs offer greater biodegradability and can represent more environmentally benign alternatives in many applications.[6]

The NMR data (Figures S1−S9) agree well with the chemical structures (Figure 1). First, the alkyl chain directly
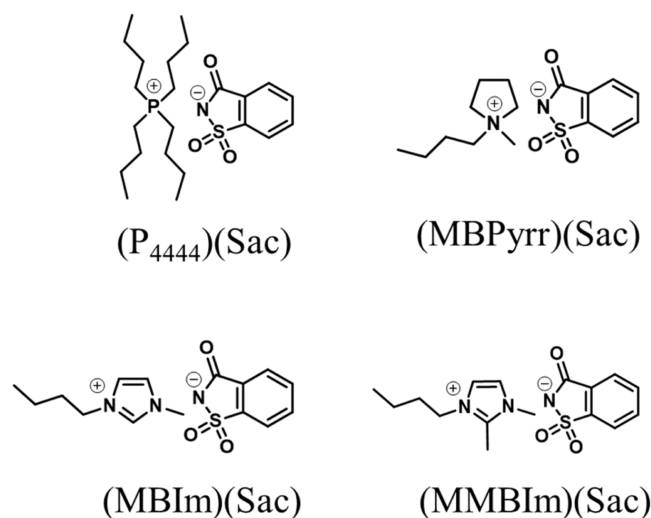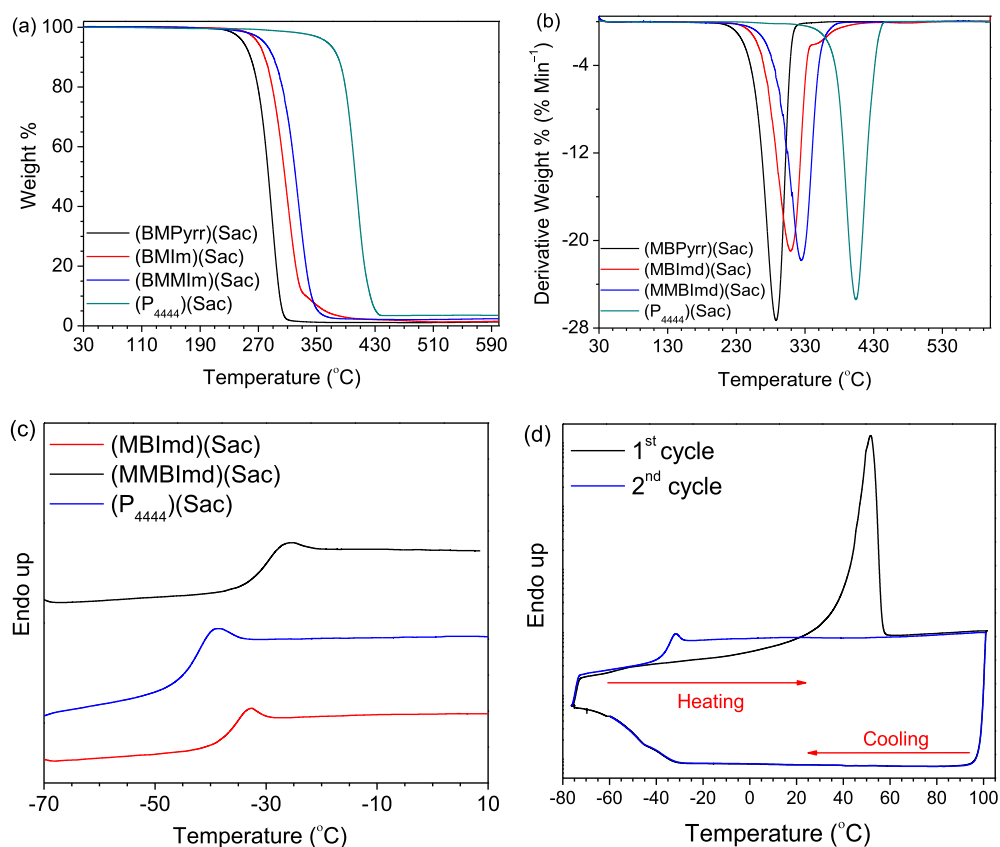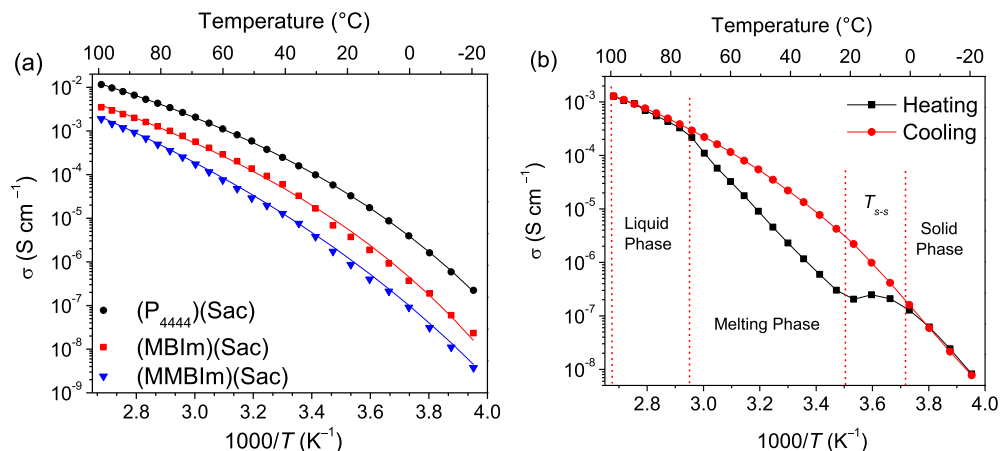

Figure 1. Chemical structures and acronyms of the four ILs.

Figure 2. TGA thermograms (a), DTG curves (b), DSC traces for the RTILs (c), and (MBPyrr)(Sac) (d). The DSC traces in (c) are shifted along the Y-axis for clarity.


Figure 3. Ionic conductivity of the RTILs, heating cycles (a), for (MBPyrr)(Sac), both heating and cooling cycles (b), as a function of temperature. The solid lines indicate the best fit of the data to the VFT equation for the heating cycle data of (a) and cooling cycle data of (b).

attached to the charged heteroatom of cation gives characteristic ^{1}H NMR resonance lines in the aliphatic region: a triplet for terminal methyl group at 0.8−0.9 ppm, multiplets at 1.2−1.3 and 1.7−1.8 ppm for methylene protons, and a triplet at ca. 4.2 ppm for the methylene proton next to the heteroatom. Second, the presence of an aromatic signal in the region of 7−8 ppm confirms the metathesis reaction and formation of the ILs. Third, the presence of ^{13}C NMR resonance lines in the range 10−50 ppm corresponds to aliphatic groups of the cations, while those at 120−150 ppm the anion aromatic ring, and the carbonyl signal at ca. 170 ppm, together with the ^{31}P resonance

line at 33 ppm for (P$_{4444}$)(Sac), further confirms the purity of the ILs.

Thermal Properties. Dynamic TGA reveals all ILs to be stable up to >260 °C with a simple single-step decomposition (Figure 2a), as further supported by derivative thermogravimetry (DTG) data (Figure 2b). Yet, these stabilities are slightly overestimated as only isothermal TGA can assess long-term thermal stability.[33,34] (P$_{4444}$)(Sac) shows the best thermal stability while (MBPyrr)(Sac) displays the worst, and overall, the ILs with C-2 methylated imidazolium cations have relatively better thermal stabilities than those with unmethylated cations, due to carbene formation.[35] Overall, the thermal
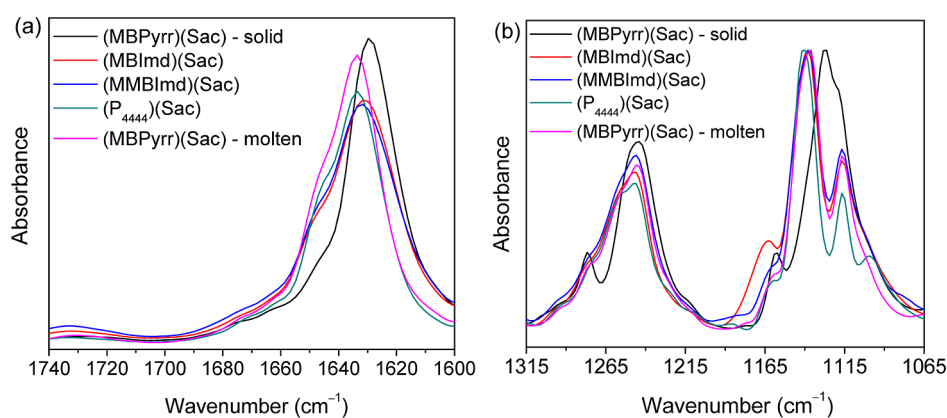
Figure 4. FTIR spectra of the ILs: −CO region (a); −SO$_2$ region (b).

stabilities are worse than those of the corresponding TFSI-based ILs.[36−38]

The first DSC heating cycle of (MBPyrr)(Sac) shows a glass transition, T_g, and a broad thermal event, ranging from 20 to 60 °C. The latter is too broad for a single simple process but is most likely due to multiple solid−solid phase transitions (T_{s-s}) followed by a melting (T_m) (Figure 2d, Table 1). During the second heating cycle, no other thermal event was found except a T_g (Figures 2d and S10), indicating an irreversible thermal behavior within the short period of time. To try to further resolve the broad thermal event, we used a 2 °C min^{-1} scan rate, but no obvious differences were observed (Figure S11).

All of the RTILs exhibited only glass transition temperatures (T_g) and behaved as glassy liquids (Figure 2c). The T_g increases from (P$_{4444}$)(Sac) to (MBIm)(Sac) and (MMBIm)-(Sac). For the imidazolinium-based ILs, with a methyl group at the C-2 position, the higher T_g likely comes from stronger $\pi-\pi$ and dispersion interactions. As compared to its fluorinated analogues, (MBPyrr)(Sac) shows a ca. 40 K higher melting point.[39,40] Similarly, (MMBPyrr)(Sac) and (MBPyrr)(Sac) show higher T_g than their TFSI analogues.[41]

Ionic Conductivity. As expected, the ionic conductivities of the RTILs increase as a function of the temperature (Figure 3a). (P$_{4444}$)(Sac) exhibited higher ionic conductivities than the imidazolinium analogues, demonstrating better ion−ion dissociation than that for the N-based ILs and correlating well with the DSC data. Indeed, an additional methyl group at the C-2 position of the imidazolinium cation causes a significant drop in the ionic conductivity due to increased ion−ion interactions. As compared to its fluorinated analogues, the ionic conductivities of the (MBIm)(Sac) and (MMBIm)-(Sac) ILs are lower throughout the whole studied temperature range,[41] possibly due to stronger ion−ion interactions from and alongside symmetry and conformational restrictions of the Sac anion. However, the reverse behavior for (P$_{4444}$)(Sac), with significantly improved ionic conductivity as compared to its TFSI analogue,[38] may be due to decreased ion−ion interactions; this is because the Sac anion tautomerism causes its negative charge to be more localized on the oxygen atom than on the nitrogen atom, due to the electronegativity of oxy, and oxygen has a stronger affinity for phosphorus than nitrogen does (Lewis hard acid−base rule).

In contrast to the three RTILs, the ionic conductivity of the (MBPyrr)(Sac) IL, a solid at RT, increases upon heating between −20 °C and ca. 0 °C and then remains almost unchanged until 15 °C, consistent with the T_{s-s} transitions,

possibly caused by distinct polymorphs and disorder in the crystalline state, which agrees well with the DSC data (Figures 3b and S10). Subsequently, a notable increase in ionic conductivity is observed between 15 and 75 °C, likely connected to elongated melting, and finally the IL behaves entirely like a liquid above 75 °C. In stark contrast, during cooling, (MBPyrr)(Sac) behaves like a liquid, and no transitions are observed, which again corroborates well with the DSC data and confirms its supercooled liquid nature.

The E_σ obtained from the VFT fitting, follows the order: (P$_{4444}$)(Sac)>(MBIm)(Sac)> (MMBIm)(Sac) (Table S1), again in accordance with the DSC data and again indicates a reduction in the number of charge carriers by ion−ion interactions via σ_0. The T_0 are all consistent with the DSC thermal behavior, and the empirical approximation: $T_0/T_g \approx$ 0.75, often used for ILs.[3]

Ion−Ion Interactions. The influence of ion−ion interactions on the overall physicochemical properties is mainly monitored using FTIR spectroscopy via the −CO and −SO$_2$ stretching vibrations of the Sac anion (Figure 4). For (MBPyrr)(Sac), in its solid state, the CO band appears as a strong symmetrical band with a weak shoulder centered at ca. 1630 cm^{-1} (Figure 4a), a band that is shifted toward higher wavenumbers by ca. 10 cm^{-1} together with a stronger shoulder for all the RTILs and (MBPyrr)(Sac) in the molten state, indicating a symmetry-induced splitting,[42] most prominent for (P$_{4444}$)(Sac). In the SO$_2$ group stretching region, there are two bands for (MBPyrr)(Sac); the asymmetric at 1245 cm^{-1} with small shoulders on both sides and the symmetric at 1126 cm^{-1} with a shoulder toward higher wavenumbers, which is quite similar to the spectral features of Na$_3$Sac$_3$,[43] implying the presence of a single type of −SO$_2$ group and also suggests that it may exist as the trimeric form, which would justify its higher melting point than the other Sac ILs (Figure 4b). The RTILs and molten (MBPyrr)(Sac) shift the SO$_2$ symmetric bands to higher wavenumbers, together with well-resolved shoulders, while the asymmetric band is most affected for (P$_{4444}$)(Sac), suggesting two or more types of SO$_2$ group interactions, which clearly points toward different delocalized conformers of the Sac anion also being heavily dependent on the nature of the IL cations. This further supports its low glass transition temperature and the high ionic conductivity of (P$_{4444}$)(Sac).

Electrochemical Assessment. First, (P$_{4444}$)(Sac) exhibited a much wider ESW, 6.0 V, than the imidazolium-based ILs, (MMBIm)(Sac) and (MBIm)(Sac), at 4.5 and 4.2 V, respectively (Figure 5). This is most likely due to the
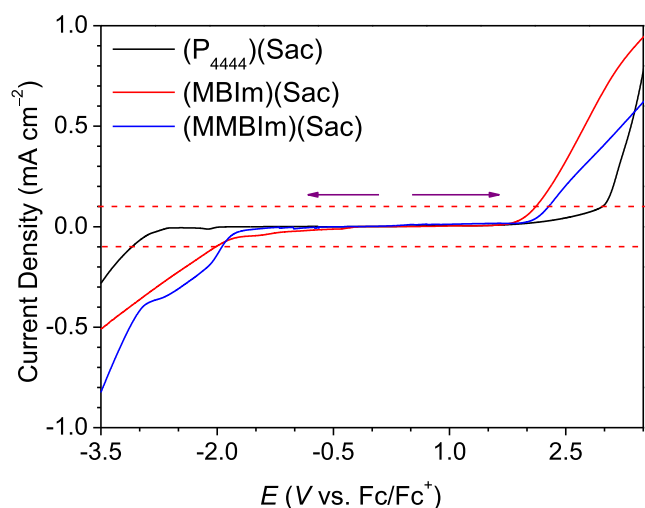
Figure 5. LSV using GC as a WE at 20 °C.

electrochemical stability of the quaternary phosphonium cation. The imidazolinium cation-based ILs have almost the same cathodic limits, but the MBIm cation-based IL has a lower anodic limit, which is due to the oxidative decomposition at the C-2 carbon. Overall, these ILs exhibit large ESWs not only as compared to other fluorine-free ILs[14,44] but also ESWs wider and/or on par with their fluorinated analogues.[3]

Due to its thermal and electrochemical stabilities, (P_{4444})-(Sac) was selected as the electrolyte for further SC tests. The initial tests showed elevated temperatures to improve the SC performance, which can be attributed to a higher ionic conductivity and faster ion diffusion . As expected the specific capacitance decreases with increased scan rate, whereas it increases as a function of temperature (Figures 6, S12, S13, and Table S2).[40,41]

(P_{4444})(Sac) demonstrates a typical capacitive response, where the slower scan rates produce a significant peak current,[41,45] but the faster scan rates do not allow the system to establish equilibrium, making the charging and discharging of the double layer less obvious and resulting in a decline in the peak current.[32,46]

The Nyquist plot from the EIS data consists of a semicircle in the upper-frequency domain, a linear variation at a midrange

frequency, and a developing vertical tail in the lower-frequency domain as the temperature increases from 30 to 60 °C (Figure S14).[47,48] Typically, a rapid migration of ions occurs at the surface of electrode in the higher frequency domain.[49,50] The ions spend more time at the electrode interface at the lower frequency domain, thus growing the vertical end.[51] The semicircle thus indicates resistance due to the charge transfer at the electrode−electrolyte interface, demonstrating the presence of electrolyte ions at the surface of the electrodes as a result of interfacial contact between the electrode surfaces, the current collectors, and the electrolyte.[46,52]

The charge−discharge performance shows that during the discharge period at higher current densities, the device exhibits an IR drop, which might be a result of the high viscosity and large pore size of (P_{4444})(Sac) ions than the electrode material (Figures 7 a,b and S15).[12] The long-term cyclic stability exhibits some distortions during the initial cycles, likely due to the initial internal resistance, but the stability improves in subsequent cycles, and the device demonstrates typical double-layer capacitance behavior (Figure 7c).[12] The capacitor retained 81% and 60% of its initial capacitance after 10,000 cycles at 60 and 30 °C, respectively (Figure 7d), which is on par with the previous studies using fluorinated ILs.[53−55] This indicates that at 60 °C, the (P_{4444})(Sac) maintains sufficient fluidity for effective ion mobility and significant ion accumulation on the electrode surface; however, both fluidity and ion accumulation decrease at lower temperatures.[12,56] Moreover, the SC showed a Coulombic efficiency of 94% (at 30 °C) and 96% (at 60 °C) after 5000 and 10,000 charge−discharge cycles, respectively. In addition, a specific energy density of roughly 53 Wh kg^{-1} and a power density of 300 W kg^{-1} at a current density of 0.1 A g^{-1} and 60 °C are possible due to the high thermal and electrochemical stability along with the wide potential window of the (P_{4444})(Sac).

■ CONCLUSIONS

Out of the four new ILs presented, it is clear that (P_{4444})(Sac) has beneficial physicochemical and electrochemical properties, including better thermal stability, lower glass transition temperature, higher ionic conductivity, and at least a 1.5 V wider ESW than its imidazolium/pyrrolidinium analogues. For all the four ILs, the ion−ion interactions are greatly influenced by the different coordination modes of the Sac anion, which are, in turn, affected by the chemical structure, size, and nature
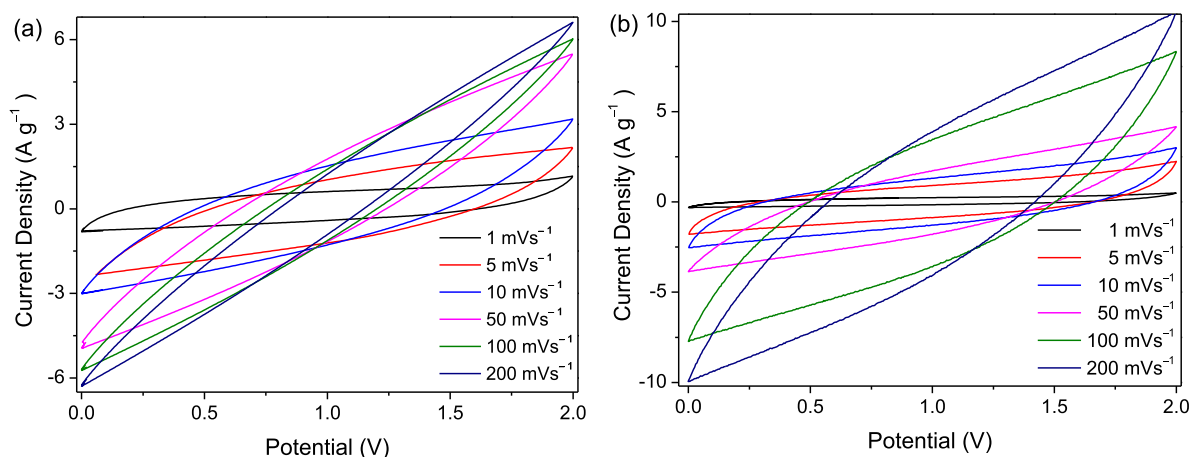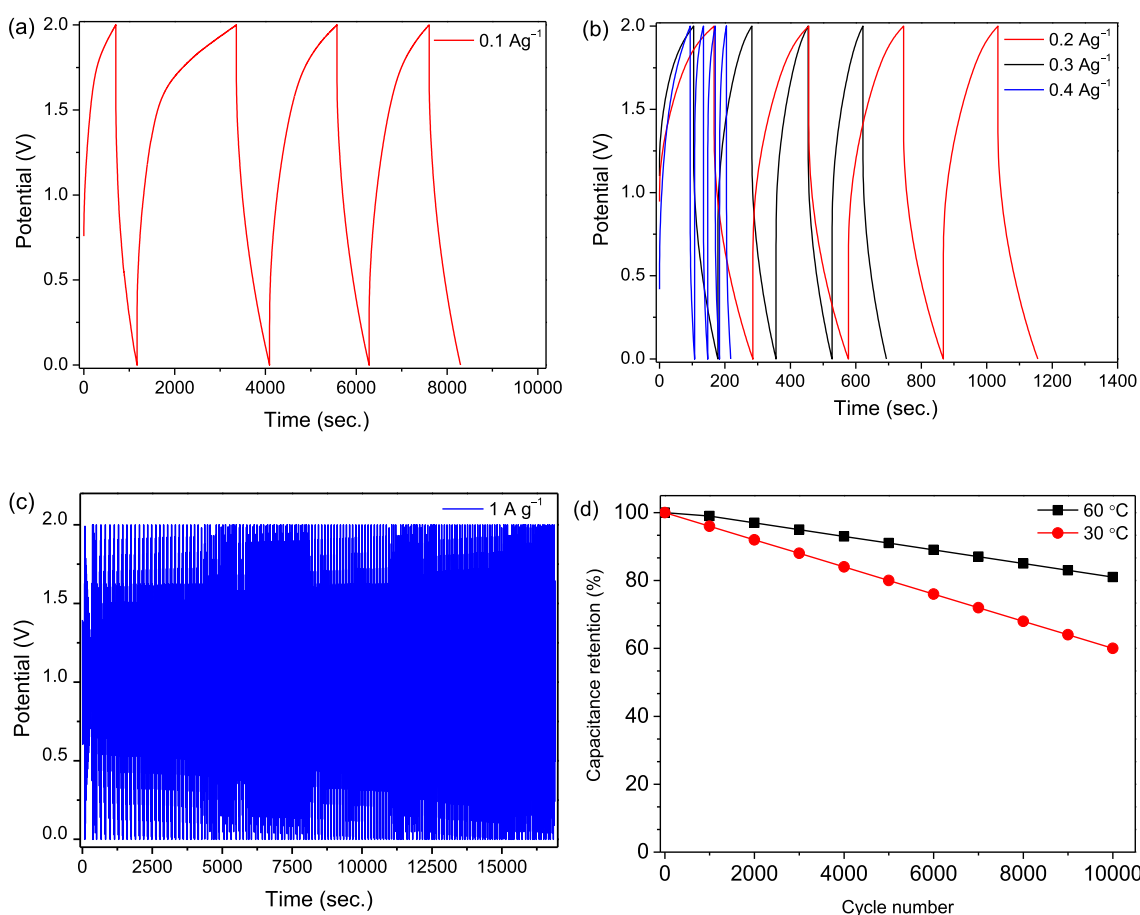

Figure 6. (a) CV plots of (P_{4444})(Sac) with different scan rates at 30 °C and (b) 60 °C.

Figure 7. GCD plots (a,b), cyclic stability for 10,000 cycles (c), and capacitance retention after 10,000 cycles at 30 and 60 °C (d) of $(P_{4444})(Sac)$.

of the counterion—the smaller pyridinium cation interacts stronger and the bulkier (P_{4444}) cation more weakly. The $(P_{4444})(Sac)$ IL exhibited efficient charge storage performance as an electrolyte in a symmetric supercapacitor, in particular, at somewhat elevated temperatures, which is needed to improve the ionic conductivity by reduced viscosity. Overall, this study demonstrated that even fluorine-free and "greener" ILs can potentially be used as SC electrolytes, with a promise to fully or partly replace the more popular TFSI-anion-based ILs and electrolytes in next-generation energy storage devices.

ASSOCIATED CONTENT

ⓢ Supporting Information

The Supporting Information is available free of charge at https://pubs.acs.org/doi/10.1021/acssuschemeng.4c06290.

> NMR spectra; DSC traces and ionic conductivity; CV plots; specific capacitance; Nyquist plots; GCD plots; cyclic stability; table of VFT equation parameters and apparent ionic conductivity activation energies; and table of specific capacitances, energy densities, and power densities (PDF)

AUTHOR INFORMATION

Corresponding Authors

Patrik Johansson − *Department of Physics, Chalmers University of Technology, SE-412 96 Gothenburg, Sweden;* ⓞ orcid.org/0000-0002-9907-117X; Email: patrik.johansson@chalmers.se

Faiz Ullah Shah − *Chemistry of Interfaces, Luleå University of Technology, SE-971 87 Luleå, Sweden;* ⓞ orcid.org/0000-0003-3652-7798; Email: faiz.ullah@ltu.se

Authors

Mukhtiar Ahmed − *Chemistry of Interfaces, Luleå University of Technology, SE-971 87 Luleå, Sweden*

Gaurav Tatrari − *Chemistry of Interfaces, Luleå University of Technology, SE-971 87 Luleå, Sweden;* ⓞ orcid.org/0000-0002-9953-8075

Complete contact information is available at:
https://pubs.acs.org/10.1021/acssuschemeng.4c06290

Notes

The authors declare no competing financial interest.

REFERENCES

(1) Walden, P. Molecular weights and electrical conductivity of several fused salts. *Bull. Acad. Imp. Sci. St.-Petersbourg* **1914**, *1800*, 405−422.

(2) MacFarlane, D. R.; Tachikawa, N.; Forsyth, M.; Pringle, J. M.; Howlett, P. C.; Elliott, G. D.; Davis, J. H.; Watanabe, M.; Simon, P.; Angell, C. A. Energy applications of ionic liquids. *Energy Environ. Sci.* **2014**, *7* (1), 232−250.

(3) Galiński, M.; Lewandowski, A.; Stępniak, I. Ionic liquids as electrolytes. *Electrochim. Acta* **2006**, *51* (26), 5567−5580.

(4) Carter, E. B.; Culver, S. L.; Fox, P. A.; Goode, R. D.; Ntai, I.; Tickell, M. D.; Traylor, R. K.; Hoffman, N. W.; Davis, J. H. Sweet success: ionic liquids derived from non-nutritive sweeteners. *Chem. Commun.* **2004**, *35* (27), 630.

(5) Lei, Z.; Chen, B.; Koo, Y.-M.; MacFarlane, D. R. Introduction: Ionic Liquids. *Chem. Rev.* **2017**, *117*, 6633−6635.

(6) Vieira, N. S.; Stolte, S.; Araujo, J. M.; Rebelo, L. P. N.; Pereiro, A. B.; Markiewicz, M. Acute aquatic toxicity and biodegradability of fluorinated ionic liquids. *ACS Sustainable Chem. Eng.* **2019**, *7* (4), 3733−3741.

(7) Swatloski, R. P.; Holbrey, J. D.; Rogers, R. D. Ionic liquids are not always green: hydrolysis of 1-butyl-3-methylimidazolium hexa-fluorophosphate. *Green Chem.* **2003**, *5* (4), 361.

(8) Scheers, J.; Lim, D.-H.; Kim, J.-K.; Paillard, E.; Henderson, W. A.; Johansson, P.; Ahn, J.-H.; Jacobsson, P. All fluorine-free lithium battery electrolytes. *J. Power Sources* **2014**, *251*, 451−458.

(9) Simon, P.; Gogotsi, Y. Perspectives for electrochemical capacitors and related devices. *Nat. Mater.* **2020**, *19* (11), 1151−1163.

(10) Simon, P.; Gogotsi, Y. Materials for electrochemical capacitors. *Nat. Mater.* **2008**, *7* (11), 845−854.

(11) Candelaria, S. L.; Shao, Y.; Zhou, W.; Li, X.; Xiao, J.; Zhang, J.-G.; Wang, Y.; Liu, J.; Li, J.; Cao, G. Nanostructured carbon for energy storage and conversion. *Nano energy* **2012**, *1* (2), 195−220.

(12) Khan, I. A.; Shah, F. U. Fluorine-free ionic liquid-based electrolyte for supercapacitors operating at elevated temperatures. *ACS Sustainable Chem. Eng.* **2020**, *8* (27), 10212−10221.

(13) Ahmed, M.; Filippov, A.; Johansson, P.; Shah, F. U. Pyrrolidium-and Imidazolium-Based Ionic Liquids and Electrolytes with Flexible Oligoether Anions. *ChemPhysChem* **2024**, *25* (9), No. e202300810.

(14) Bhowmick, S.; Filippov, A.; Khan, I. A.; Shah, F. U. Physical and electrochemical properties of new structurally flexible imidazo-lium phosphate ionic liquids. *Phys. Chem. Chem. Phys.* **2022**, *24* (38), 23289−23300.

(15) Liew, C.-W.; Ramesh, S. Comparing triflate and hexafluor-ophosphate anions of ionic liquids in polymer electrolytes for supercapacitor applications. *Materials* **2014**, *7* (5), 4019−4033.

(16) Jain, P.; Antzutkin, O. N. Nonhalogenated surface-active ionic liquid as an electrolyte for supercapacitors. *ACS Appl. Energy Mater.* **2021**, *4* (8), 7775−7785.

(17) Jain, P.; Antzutkin, O. N. 2-Ethylhexylsulfate Anion-based Surface-Active Ionic Liquids (SAILs) as temperature persistent electrolytes for supercapacitors. *J. Ionic Liq.* **2022**, *2* (2), 100034.

(18) Zhang, W.; Zhang, F.; Zhang, P.; Liang, S.; Shi, Z. N-Propyl-N-Methylpyrrolidinium Difluoro (oxalato) borate as a Novel Electrolyte for High-Voltage Supercapacitor. *Front. Chem.* **2019**, *7*, 664.

(19) Abdallah, T.; Lemordant, D.; Claude-Montigny, B. Are room temperature ionic liquids able to improve the safety of supercapacitors organic electrolytes without degrading the performances? *J. Power Sources* **2012**, *201*, 353−359.

(20) Bešter-Rogač, M.; Stoppa, A.; Buchner, R. Ion association of imidazolium ionic liquids in acetonitrile. *J. Phys. Chem. B* **2014**, *118* (5), 1426−1435.

(21) White, S. R. Chemistry and controversy: regulating the use of chemicals in foods, 1883−1959. Ph.D. Thesis, Emory University, 1994.

(22) Gouveia, A. S.; Bernardes, C. E.; Tomé, L. C.; Lozinskaya, E. I.; Vygodskii, Y. S.; Shaplov, A. S.; Lopes, J. N. C.; Marrucho, I. M. Ionic liquids with anions based on fluorosulfonyl derivatives: from asymmetrical substitutions to a consistent force field model. *Phys. Chem. Chem. Phys.* **2017**, *19* (43), 29617−29624.

(23) Foropoulos, J.; DesMarteau, D. D. Synthesis, properties, and reactions of bis ((trifluoromethyl) sulfonyl) imide,(CF3SO2) 2NH. *Inorg. Chem.* **1984**, *23* (23), 3720−3723.

(24) Kulkarni, P. S.; Branco, L. C.; Crespo, J. G.; Nunes, M. C.; Raymundo, A.; Afonso, C. A. Comparison of physicochemical properties of new ionic liquids based on imidazolium, quaternary ammonium, and guanidinium cations. *Chem.—Eur. J.* **2007**, *13* (30), 8478−8488.

(25) Li, Z.; Pei, Y.; Wang, H.; Fan, J.; Wang, J. Ionic liquid-based aqueous two-phase systems and their applications in green separation processes. *TrAC, Trends Anal. Chem.* **2010**, *29* (11), 1336−1346.

(26) Greer, A. J.; Jacquemin, J.; Hardacre, C. Industrial applications of ionic liquids. *Molecules* **2020**, *25* (21), 5207.

(27) Armand, M.; Johansson, P. Novel weakly coordinating heterocyclic anions for use in lithium batteries. *J. Power Sources* **2008**, *178* (2), 821−825.

(28) Armand, M.; Johansson, P.; Bukowska, M.; Szczeciński, P.; Niedzicki, L.; Marcinek, M.; Dranka, M.; Zachara, J.; Żukowska, G.; Marczewski, M.; et al. Review—Development of Hückel Type Anions: From Molecular Modeling to Industrial Commercialization. A Success Story. *J. Electrochem. Soc.* **2020**, *167* (7), 070562.

(29) Canongia Lopes, J. N.; Pádua, A. A. H. Molecular force field for ionic liquids III: Imidazolium, pyridinium, and phosphonium cations; chloride, bromide, and dicyanamide anions. *J. Phys. Chem. B* **2006**, *110* (39), 19586−19592.

(30) Bandrés, I.; Montano, D. F.; Gascón, I.; Cea, P.; Lafuente, C. Study of the conductivity behavior of pyridinium-based ionic liquids. *Electrochim. Acta* **2010**, *55* (7), 2252−2257.

(31) Tatrari, G.; Karakoti, M.; Tewari, C.; Pandey, S.; Bohra, B. S.; Dandapat, A.; Sahoo, N. G. Solid waste-derived carbon nanomaterials for supercapacitor applications: a recent overview. *Mater. Adv.* **2021**, *2* (5), 1454−1484.

(32) Zhang, S.; Pan, N. Supercapacitors performance evaluation. *Adv. Energy Mater.* **2015**, *5* (6), 1401401.

(33) Shah, F. U.; Khan, I. A.; Johansson, P. Comparing the thermal and electrochemical stabilities of two structurally similar ionic liquids. *Molecules* **2020**, *25* (10), 2388.

(34) Oltean, G.; Plylahan, N.; Ihrfors, C.; Wei, W.; Xu, C.; Edström, K.; Nyholm, L.; Johansson, P.; Gustafsson, T. Towards Li-Ion Batteries Operating at 80 °C: Ionic Liquid versus Conventional Liquid Electrolytes. *Batteries* **2018**, *4* (1), 2.

(35) Holloczki, O.; Gerhard, D.; Massone, K.; Szarvas, L.; Nemeth, B.; Veszprémi, T.; Nyulaszi, L. Carbenes in ionic liquids. *New J. Chem.* **2010**, *34* (12), 3004.

(36) Behrens, M.; Cross, J. S.; Akasaka, H.; Ohtake, N. Pyrolysis of cellulose mixed with ionic liquids 1-butyl-3-methylimidazolium bis (trifluoromethylsulfonyl) imide [bmim] [TFSI], 1-butyl-3-methyl-imidazolium tetrafluoroborate [bmim] [BF4], and 1-butyl-2, 3-dimethylimidazolium tetrafluoroborate [bmmim] [BF4]. *Biomass Bioenergy* **2019**, *122*, 290−297.

(37) Shamsipur, M.; Beigi, A. A. M.; Teymouri, M.; Pourmortazavi, S. M.; Irandoust, M. Physical and electrochemical properties of ionic liquids 1-ethyl-3-methylimidazolium tetrafluoroborate, 1-butyl-3-methylimidazolium trifluoromethanesulfonate and 1-butyl-1-methyl-pyrrolidinium bis (trifluoromethylsulfonyl) imide. *J. Mol. Liq.* **2010**, *157* (1), 43−50.

(38) Wu, F.; Schür, A. R.; Kim, G.-T.; Dong, X.; Kuenzel, M.; Diemant, T.; D'Orsi, G.; Simonetti, E.; De Francesco, M.; Bellusci, M.; et al. A novel phosphonium ionic liquid electrolyte enabling high-voltage and high-energy positive electrode materials in lithium-metal batteries. *Energy Storage Mater.* **2021**, *42*, 826−835.

(39) Macfarlane, D. R.; Meakin, P.; Sun, J.; Amini, N.; Forsyth, M. Pyrrolidinium imides: a new family of molten salts and conductive plastic crystal phases. *J. Phys. Chem. B* **1999**, *103* (20), 4164−4170.

(40) Furlani, M.; Albinsson, I.; Mellander, B.-E.; Appetecchi, G.; Passerini, S. Annealing protocols for pyrrolidinium bis (trifluorome-thylsulfonyl) imide type ionic liquids. *Electrochim. Acta* **2011**, *57*, 220−227.

(41) Agafonov, A.; Ramenskaya, L.; Grishina, E.; Kudryakova, N. Cation effects on the properties of halloysite-confined bis (trifluoromethylsulfonyl) imide based ionic liquids. *RSC Adv.* **2021**, *11* (61), 38605−38615.

(42) Jovanovski, G. Metal saccharinates and their complexes with N-donor ligands. *Croat. Chem. Acta* **2000**, *73* (3), 843.

(43) Jovanovski, G.; Kamenar, B. Two ionic saccharinates:(la) sodium saccharinate 2/3 hydrate, C7H4NO3SNa· 2/3H2O;(lb) Magnesium disaccharinate heptahydrate,(C7H4NO3S) 2Mg· 7H2O. *Cryst. Struct. Commun.* **1982**, *11*, 247−255.

(44) Ahmed, M.; Bhowmick, S.; Filippov, A.; Johansson, P.; Shah, F. U. Ionic Liquids and Electrolytes with Flexible Aromatic Anions. *Chem.—Eur. J.* **2023**, *29* (41), No. e202301000.

(45) Khan, I. A.; Wang, Y.-L.; Shah, F. U. Effect of structural variation in biomass-derived nonfluorinated ionic liquids electrolytes on the performance of supercapacitors. *J. Energy Chem.* **2022**, *69*, 174−184.

(46) Wu, J. Understanding the electric double-layer structure, capacitance, and charging dynamics. *Chem. Rev.* **2022**, *122* (12), 10821−10859.

(47) Zhao, D.; Chen, C.; Zhang, Q.; Chen, W.; Liu, S.; Wang, Q.; Liu, Y.; Li, J.; Yu, H. High performance, flexible, solid-state supercapacitors based on a renewable and biodegradable mesoporous cellulose membrane. *Adv. Energy Mater.* **2017**, *7* (18), 1700739.

(48) Mei, B.-A.; Munteshari, O.; Lau, J.; Dunn, B.; Pilon, L. Physical interpretations of Nyquist plots for EDLC electrodes and devices. *J. Phys. Chem. C* **2018**, *122* (1), 194−206.

(49) Arulepp, M.; Permann, L.; Leis, J.; Perkson, A.; Rumma, K.; Jänes, A.; Lust, E. Influence of the solvent properties on the characteristics of a double layer capacitor. *J. Power Sources* **2004**, *133* (2), 320−328.

(50) Chen, Z.; Wen, J.; Yan, C.; Rice, L.; Sohn, H.; Shen, M.; Cai, M.; Dunn, B.; Lu, Y. High-performance supercapacitors based on hierarchically porous graphite particles. *Adv. Energy Mater.* **2011**, *1* (4), 551−556.

(51) Maity, S.; Banerjee, D.; Bhattacharya, G.; Roy, S. S.; Dhar, B. B. Hydrothermally synthesized sulfur-doped graphite as supercapacitor electrode materials. *ACS Appl. Nano Mater.* **2022**, *5* (3), 3548−3557.

(52) Noh, C.; Jung, Y. Understanding the charging dynamics of an ionic liquid electric double layer capacitor via molecular dynamics simulations. *Phys. Chem. Chem. Phys.* **2019**, *21* (13), 6790−6800.

(53) Chen, W.; Wei, Y.; Ge, X.; Li, S.; Zhang, X.; Wang, Z.-X.; Xing, Z.; Zhang, Q.; Liu, X. Insight of alkyl imidazolium tetrafluoroborate ionic gels as supercapacitors and motion sensors: Effects of alkyl chain length and intermolecular interactions. *J. Power Sources* **2024**, *599*, 234224.

(54) Shamsuri, N.; Hamsan, M.; Shukur, M.; Alias, Y.; Halim, S.; Aziz, S.; Jahidin, A.; Sulaiman, M.; Yuwana, L.; Siong, S. O. J.; et al. Enhancing EDLC applications with [BMIM] BF$_4$-integrated cellulose gel electrolyte for sustainable energy storage. *J. Energy Storage* **2024**, *75*, 109559.

(55) Zaccagnini, P.; di Giovanni, D.; Gomez, M. G.; Passerini, S.; Varzi, A.; Lamberti, A. Flexible and high temperature supercapacitor based on laser-induced graphene electrodes and ionic liquid electrolyte, a de-rated voltage analysis. *Electrochim. Acta* **2020**, *357*, 136838.

(56) Yamagata, M.; Soeda, K.; Ikebe, S.; Yamazaki, S.; Ishikawa, M. Chitosan-based gel electrolyte containing an ionic liquid for high-performance nonaqueous supercapacitors. *Electrochim. Acta* **2013**, *100*, 275−280.